



RESEARCH ARTICLE

10.1029/2022JD038408

Key Points:

- Indian Ocean contributes majority of the moisture to rainfall in the Horn of Africa drylands
- The role of vegetation and land contribution to rainfall during the short rains is increasing
- Moisture contributions are driven more by atmospheric circulation changes rather than increased evaporation from source regions

Correspondence to:

A. Koppa,
akash.koppa@ugent.be

Citation:

Koppa, A., Keune, J., MacLeod, D. A., Singer, M., Nieto, R., Gimeno, L., et al. (2023). A Lagrangian analysis of the sources of rainfall over the Horn of Africa drylands. *Journal of Geophysical Research: Atmospheres*, 128, e2022JD038408. <https://doi.org/10.1029/2022JD038408>

Received 22 DEC 2022
Accepted 12 JUN 2023







Author Contributions:

Conceptualization: Akash Koppa, Jessica Keune, Diego G. Miralles
Data curation: Akash Koppa, Raquel Nieto, Luis Gimeno
Formal analysis: Akash Koppa, Jessica Keune, Dave A. MacLeod
Funding acquisition: Diego G. Miralles
Investigation: Akash Koppa
Methodology: Akash Koppa, Jessica Keune, Diego G. Miralles
Software: Akash Koppa, Jessica Keune
Supervision: Diego G. Miralles
Validation: Akash Koppa
Visualization: Akash Koppa
Writing – original draft: Akash Koppa

© 2023 The Authors.

This is an open access article under the terms of the [Creative Commons Attribution-NonCommercial License](https://creativecommons.org/licenses/by/4.0/), which permits use, distribution and reproduction in any medium, provided the original work is properly cited and is not used for commercial purposes.

A Lagrangian Analysis of the Sources of Rainfall Over the Horn of Africa Drylands

Akash Koppa¹ , Jessica Keune¹ , Dave A. MacLeod² , Michael Singer³ , Raquel Nieto⁴ , Luis Gimeno⁴, Katerina Michaelides² , Rafael Rosolem² , George Otieno⁵, Abebe Tadege⁵, and Diego G. Miralles¹ 

¹Hydro-Climate Extremes Lab (H-CEL), Ghent University, Ghent, Belgium, ²School of Geographical Sciences, University of Bristol, Bristol, UK, ³School of Earth and Environmental Sciences, Cardiff University, Cardiff, UK, ⁴Centro de Investigación Mariñá, Environmental Physics Laboratory (EPHysLab), Universidade de Vigo, Ourense, Spain, ⁵IGAD Climate Prediction and Application Centre, Nairobi, Kenya

Abstract The Horn of Africa drylands (HAD) are among the most vulnerable regions to hydroclimatic extremes. The two rainfall seasons—long and short rains—exhibit high intraseasonal and interannual variability. Accurately simulating the long and short rains has proven to be a significant challenge for the current generation of weather and climate models, revealing key gaps in our understanding of the drivers of rainfall in the region. In contrast to existing climate modeling and observation-based studies, here we analyze the HAD rainfall from an observationally-constrained Lagrangian perspective. We quantify and map the region's major oceanic and terrestrial sources of moisture. Specifically, our results show that the Arabian Sea (through its influence on the northeast monsoon circulation) and the southern Indian Ocean (via the Somali low-level jet) contribute ~80% of the HAD rainfall. We see that moisture contributions from land sources are very low at the beginning of each season, but supply up to ~20% from the second month onwards, that is, when the oceanic-origin rainfall has already increased water availability over land. Further, our findings suggest that the interannual variability in the long and short rains is driven by changes in circulation patterns and regional thermodynamic processes rather than changes in ocean evaporation. Our results can be used to better evaluate, and potentially improve, numerical weather prediction and climate models, and have important implications for (sub-)seasonal forecasts and long-term projections of the HAD rainfall.

Plain Language Summary The drylands in the Horn of Africa (HAD) have suffered a series of droughts in recent years with the consecutive failure of both the major rainfall seasons. So far, the rainfall in this region has been studied using observations and outputs from global climate models. In contrast, here, we employ a moisture tracking model, which traces individual parcels of moisture-carrying air parcels from their destination (the HAD region) to their sources (land areas within and outside the HAD, and the oceans). We find that the majority of the moisture which causes rainfall in the HAD region comes from the oceans. However, in recent years, we see that land contributions are gaining importance in affecting water availability in the region.

1. Introduction

Rainfall in the Horn of Africa drylands (HAD)—the semi-arid and arid parts of Somalia, Ethiopia, and Kenya (Figure 1a)—is crucial for sustaining the region's predominantly rainfed agriculture and pasture-dependent livelihoods. This reliance of livelihoods on rainfall renders the region highly vulnerable to hydroclimatic extremes (particularly droughts), which frequently cascade into high levels of food insecurity and humanitarian crises, especially when compounded by social conflict and high vulnerability. The vulnerability of the HAD region has recently been evidenced by the severe impacts caused by the successive failure of the two main rainfall seasons—long (March–May, MAM) and short (October–December, OND) rains—since 2020 (FEWSNET, 2022). Likewise, an anomalously strong Indian Ocean Dipole (IOD) (Saji et al., 1999), resulting in enhanced moisture transport from the Indian Ocean, has also caused major floods during the short rains in recent years, such as the unprecedented flooding in 2019 (Nicholson et al., 2022). Furthermore, shifts in the frequency and intensity of climate extremes due to climate change are expected to exacerbate flooding, food insecurity (Brown & Funk, 2008), and human conflicts (Hsiang et al., 2013; Maystadt & Ecker, 2014). Projections of drought, on the other hand, remain highly uncertain in the region, with strong divergence among models (Haile et al., 2020). In this regard, it is imperative that our current understanding of the drivers and predictability of rainfall in the HAD

Writing – review & editing: Akash Koppa, Jessica Keune, Dave A. MacLeod, Michael Singer, Raquel Nieto, Luis Gimeno, Katerina Michaelides, Rafael Rosolem, George Otieno, Abebe Tadege, Diego G. Miralles

region is improved, which can bring novel insights and opportunities for model benchmarking. Then, if accurate and timely rainfall forecasts were available, that would help enhance preparedness and design adequate adaptation and mitigation measures.

While the interannual variability of the short rains is strongly associated with coupled ocean–atmosphere oscillations—specifically the El Niño Southern Oscillation (ENSO) and the IOD (Behera et al., 2005; MacLeod et al., 2021; Manatsa & Behera, 2013; Nicholson, 2015)—the drivers of the long rains are more complex and have been the subject of much debate. In the past four decades, the long rain season in the HAD region has exhibited a consistent drying trend, contrary to projections from global climate models, a phenomenon termed as the *East African Climate Paradox* (Rowell et al., 2015; Tierney et al., 2015; Wainwright et al., 2019). Both ocean–atmospheric teleconnections and local phenomena have been posited as plausible causes for this observed drying trend. For example, the suppression of convection over Eastern Africa is strongly linked to the warming of the tropical western Pacific Ocean and the Indian Ocean (Williams & Funk, 2011). Additionally, the strengthening zonal gradients in sea surface temperatures between Indonesia and the Central Pacific have been postulated as a significant driver (Liebmann et al., 2014). C. Funk et al. (2018) also highlighted the association of a fast-warming region in the west Pacific Ocean, termed as *Western V*, with the frequency of droughts during the long rain season, and its recent long-term drying. Meanwhile, an evaluation of instrumental and reanalysis datasets by (Vellinga & Milton, 2018) suggested that the most significant factors influencing long rains variability are: the Madden-Julian Oscillation (MJO), sea surface temperatures in the north-west Indian Ocean, and the Quasi-Biennial Oscillation. Combined, these three factors can explain up to 25% of the interannual variance in precipitation. Likewise, around 18% of the decadal drying trend in the long rains has been attributed to the variability of the MJO (Walker et al., 2020). The importance of the north-west Indian Ocean is supported by climate model experiments (MacLeod, 2019), which point to near-surface processes in the north-west Indian Ocean as a key control on long rains, particularly through changes in air humidity. MacLeod (2019) also demonstrated that the south-west Indian Ocean emerges as a dominant control on May rainfall, highlighting the influential role of Somali jet variability. This strong intraseasonal variability was also highlighted by E. Dyer and Washington (2021) who diagnosed heterogeneous processes occurring throughout the season after dividing the 3 months into four discrete periods.

To date, most studies on the long and short rain seasons in the HAD region have focused on identifying relevant ocean–atmospheric teleconnections. However, very few studies have analyzed the origins of HAD rainfall in terms of moisture sources and their variability (Nieto et al., 2014). Insight into moisture sources can be provided with Lagrangian atmospheric transport models, which are widely used to identify the local and external sources of moisture contributing to rainfall over specific regions (Keune et al., 2022; Sodemann et al., 2008; Stohl et al., 2005). These models have highlighted, for instance, the critical importance of land evaporation in sustaining rainfall over different river basins around the world (Drumond et al., 2008; Fremme & Sodemann, 2019; Keune & Miralles, 2019; Sorí et al., 2018). Lagrangian models have also been useful in understanding not only the role of moisture transport in exacerbating droughts (García-Herrera et al., 2019; Herrera-Estrada et al., 2019; Holgate et al., 2020), but also their downwind impacts, which enhances spatial drought propagation (Schumacher et al., 2022), heatwave aggravation (Schumacher et al., 2019), and a cascading of ecological impacts (Zemp et al., 2017). Several studies have traced the origin of rainfall occurring over various regions in sub-Saharan Africa. For example, local evaporation was found to be an essential source of moisture for rainfall over the western Sahel (Nieto et al., 2006). Local moisture recycling has also been shown to sustain the Congo rainforest (E. L. E. Dyer et al., 2017), potentially leading to its expansion in the future (Staal et al., 2020). Salih et al. (2015) used Lagrangian models to identify Central Africa and the Arabian Peninsula as the regions with the largest contribution to the Sahelian-Sudan summer rainfall. Lagrangian models have also proved useful to unravel pathways by which moisture is transported to the West African Monsoon system (Niang et al., 2020). Despite the existence of these studies for other sub-Saharan regions, little is documented about the moisture source regions of rainfall over HAD, and the relative importance of land and oceanic moisture contributions to the trends in the long and short rains in the region.

In this study, we aim to close this research gap through the application of a Lagrangian atmospheric transport model to identify the source regions which contribute moisture during the two HAD rainfall seasons. Specifically, we seek to quantify the relative importance of oceanic and terrestrial sources of moisture for the long and short rains during normal and extreme seasons. Then, for each rainfall season, we illustrate the differences in the source regions between anomalously wet and dry years, and study the possible upwind causes explaining the changes in the moisture supply for rainfall. This study represents a step toward improving our understanding of the drivers

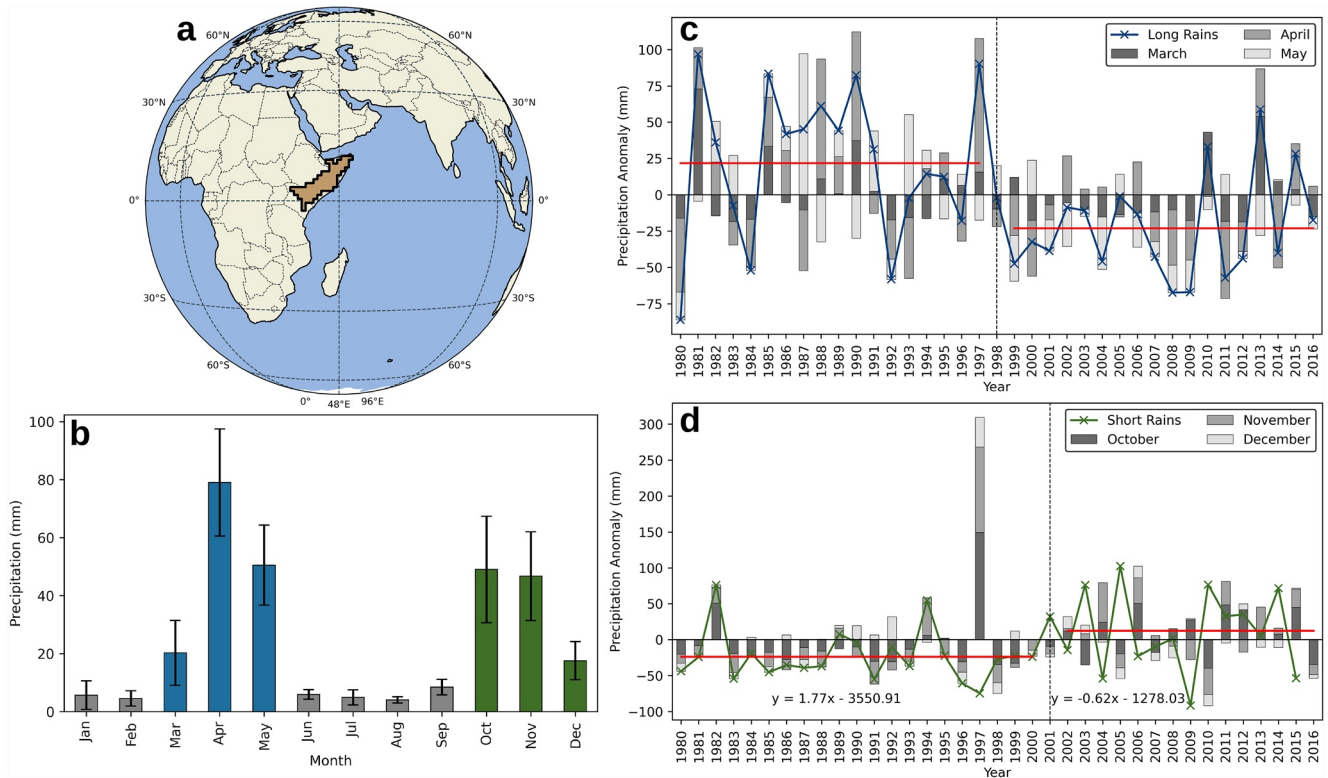


Figure 1. (a) Horn of Africa drylands (HAD). (b) Average annual cycle of rainfall in the HAD region, averaged over 1980–2016, indicating the two most important seasons, that is, the long rain season from March–May (blue) and the short rain season from October–December (green). (c) and (d) Time series of rainfall anomalies during the long and short rains respectively over the HAD region from 1980 to 2016. Dashed lines represent the change point based on Pettitt's test. The red lines represent the mean precipitation anomalies for the time periods before and after the changed point. The rainfall during the short rains in 1997 was not considered in the calculation of the mean anomalies due to the exceptional nature of ENSO.

of the recent and future interannual changes in the long and short rains using Lagrangian analysis. Furthermore, accurately delineating the source regions of moisture can aid in a more efficient selection of rainfall predictors for seasonal forecasting, and thus may potentially enable more accurate forecasts in the region (Demam et al., 2022).

2. Methods and Data

2.1. Quantification of Rainfall Moisture Sources

Lagrangian identification and quantification of the source region of rainfall over a specific “sink” region (HAD in this case) consist of two main phases. In the first phase, the output of a Lagrangian atmospheric transport model is used to track air parcels over the HAD backward in time, that is, from the sink to the source regions. In the next phase, the Lagrangian trajectories are evaluated to track the changes in moisture of the air parcels as they travel from the source regions to the sink region. In this section, we first describe the Lagrangian atmospheric transport model used in the study and then detail the moisture tracking framework used to evaluate the air parcels.

2.1.1. Lagrangian Model Simulations

The Lagrangian transport model used in this study is the Flexible Particle Dispersion model (FLEXPART) version 9.01 (Stohl et al., 2005) driven with reanalysis data (Dee et al., 2011). The model simulations are carried out at a global scale using approximately two million air parcels (each with a total air parcel mass of 2.54×10^{12} kg) which are uniformly distributed throughout the globe and are tracked both in space and time. We note that air parcels in FLEXPART are volumes of air which can be assigned all the dynamic and thermodynamic properties of atmospheric air such as specific humidity, temperature, potential temperature, and density. The following variables are used to force FLEXPART: temperature, specific humidity, horizontal and vertical wind, cloud cover, precipitation, 2-m air temperature, dew-point temperature, sensible and latent heat fluxes, and North/South and

West/East surface stress. FLEXPART tracks the location (latitude, longitude, and height) of each of the 2 million parcels and simulates their dynamic and thermodynamic properties (temperature, density, specific humidity). Using ERA-Interim data (both 6-hourly reanalysis and 3-hourly forecasts) as forcing (see below), FLEXPART model outputs are available at 3-hourly timesteps, but we only use 6-hourly reanalysis to construct the source–sink relationships.

2.1.2. Identification and Quantification of Rainfall Moisture Sources

Outputs from FLEXPART are used to construct and evaluate the trajectories of air parcels, that is, all air parcels residing over the HAD region are tracked backward in time and parsed for precipitation in the sink (HAD) region to identify moisture sources in previous time steps and locations. In doing so, all the locations in which the air parcel gains or loses moisture are traced. In this study, the evaluation of air parcel trajectories from the FLEXPART simulations are carried out using a recently developed moisture tracking framework (Keune et al., 2022). Within the framework, the trajectories are evaluated using a three-step process consisting of diagnosis, attribution, and bias-correction, as described below.

In the diagnosis step, a dataset of process (rainfall and evaporation) detection is generated by evaluating *all* global two-step trajectories. Thus, for every air parcel and every time step in the global FLEXPART simulations, precipitation (P) and evaporation (E) are detected from changes in specific humidity based on the following mass balance:

$$e - p = m * \Delta q \quad (1)$$

where, e and p (both in kg) represent net gains and losses in specific humidity for each parcel from evaporation and precipitation, respectively. m is the mass of the parcel (kg). Δq is the change in specific humidity (kg.kg^{-1}) of the parcel between two consecutive time steps along a parcel's trajectory. A parcel is assumed to contribute to a rainfall event if it undergoes a net loss of specific humidity between consecutive time steps ($\Delta q_i < 0$) and the mean relative humidity (RH) is higher than 80% (Sodemann et al., 2008), following the convection parameterization by Emanuel (1991). Then, rainfall (P in $\text{kg.kg}^{-1}.\text{m}^{-2}$) over the surface area of the sink region (A in m^2) can be estimated by integrating over individual contributions of all the air parcels n as

$$P = \frac{1}{A} \sum_i^n \Delta q_i (\Delta q_i < 0 \text{ kg.kg}^{-1}, RH_i > 80\%) \quad (2)$$

Similarly, E ($\text{kg.kg}^{-1}.\text{m}^{-2}$) is identified if the air parcel experiences a net gain of specific humidity between two consecutive time steps ($\Delta q > 0$) and the parcel resides within the atmospheric boundary layer (ABL). Integrating contributions from every air parcel, E over an area (A) is estimated as:

$$E = \frac{1}{A} \sum_i^n \Delta q_i (\Delta q_i > 0 \text{ kg.kg}^{-1}, z_i < h_{ABL}^{max}) \quad (3)$$

where, z_i is the height of the parcel (m) and h_{ABL}^{max} is the maximum height of the ABL between the two time steps considered. Finally, the accuracy and reliability of the P and E detection is evaluated using multiple criteria (details in Keune et al. (2022)).

In the attribution step, the detection criteria ($RH_i > 80\%$ and h_{ABL}^{max}) detailed above are used to evaluate the air parcels that reside over the HAD region (Figure 1). Specifically, every parcel within the HAD region which satisfies the P detection criteria, indicating rainfall, is tracked back in time for a maximum of 15 days, which includes the long tail of the distribution of the residence time of atmospheric water vapor (Sodemann, 2020). All moisture gains and losses experienced by the parcel along its trajectory are identified. Then, a quantitative attribution of evaporation in the source region to rainfall in the sink region (HAD in this case) is carried out. This is a non-trivial task as the moisture uptake experienced by the air parcel can be lost as rain *en route* to the sink region, and rain events have to be discounted using objective criteria. Here, we adopt the method of linear discounting proposed by Sodemann et al. (2008) which assumes that the air is well-mixed at all times. Therefore, it is assumed that the moisture lost at a particular time step ($t = i$) in the parcel trajectory has originated from moisture taken up in previous time steps ($t < i$), and the contribution of moisture uptake to the rainfall at time step $t = i$ is proportional to the magnitude of moisture uptakes in the previous time steps. Using this method, the fractional contribution of each source region to the sink region rainfall is calculated by discounting all *en route* losses.

This procedure allows us to establish a mass-conserving source–sink relationship that describes the contribution of surface evaporation in the source region to precipitation in the sink.

Finally, biases arising from uncertainties in P and E detection criteria are corrected using the accuracy information estimated in the diagnosis step with observations of evaporation and precipitation in the source and sink regions, respectively. First, evaporation from the source region is bias-corrected using the unconditional E flux calculated using all the air parcels over the source region (from the diagnosis step) and satellite-based E . Then, the sink region rainfall over HAD is bias-corrected using observational estimates and the contributions from the different source regions are proportionally scaled. The bias-corrections are carried out on a daily timescale.

2.2. Reanalysis and Satellite-Based Data Sets

Various hydroclimatic variables from both reanalysis and satellite-based datasets are used to drive the FLEXPART Lagrangian model and bias-correct its outputs. The model is forced with ERA-Interim global reanalysis (Dee et al., 2011) at 1° spatial resolution. Variables at single and multiple model levels (60 levels) extending from the surface toward the top of the atmosphere are used. The data spans the entire globe, and is available at 1.0° spatial resolution. Here, the 6-hourly reanalysis product and the respective 3-hourly forecasts are used for a time period of 37 years (1980–2016). The choice of ERA-Interim is motivated by the requirement of multiple consistent meteorological variables, as described above. For the bias-correction of precipitation, we use the Multi-Source Weighted Ensemble Precipitation, version 2 (MSWEP v2.8) dataset (Beck et al., 2019). The MSWEP dataset, spanning a time period of 1979–present, is generated by merging the Integrated Multi-Satellite Retrievals for the Global Precipitation Measurement (IMERG) data (Huffman et al., 2015) and the ERA5 reanalysis product (Hersbach et al., 2020) using in situ observations, and it is available at a spatial resolution of 0.1° and at 3-hourly timesteps. MSWEP v2.8 is selected as it shows considerable skill over East Africa (e.g., Sahlu et al. (2017)). To bias-correct evaporation, terrestrial evaporation from the Global Land Evaporation Amsterdam Model (GLEAM) version 3.5a is used (Martens et al., 2017; Miralles et al., 2011). This dataset is available at 0.25° at daily temporal resolution, spanning the years 1980–2020. For ocean evaporation, we use the Objectively Analyzed Air-Sea Fluxes (OAF flux) dataset (Yu & Weller, 2007). The spatial and temporal resolution of OAF flux is 1° and daily, respectively, and is available for the years 1958–2019.

2.3. Change Point Detection

We employ the Pettitt test (Pettitt, 1979) to analyze whether the rainfall regime during the long and short rains has undergone an abrupt change over the study period (1980–2016) in the HAD region. The Pettitt test is a non-parametric approach to detect significant changes in the statistical behavior of a time series. The time step at which the behavior significantly changes is identified as the *change point*. Formally, one may consider a time series of random variables $Y_{t=1}, Y_{t=2}, \dots, Y_{t=T}$; according to the Pettitt test, the time series is said to have a change point at time $t = \tau$ if $Y_{t=1} \dots Y_{t=\tau}$ have a common distribution function F_1 and $Y_{t=\tau} \dots Y_{t=T}$ have a different distribution function F_2 . The Pettitt test does not make a priori assumptions about the functional forms of F_1 and F_2 . For a detailed mathematical description of the Pettitt test, we refer the readers to Rybski and Neumann (2011). In this study, the *pyHomogeneity* Python package was used to implement the test. The exceptional ENSO year 1997 has been removed from the change point analysis of the short rains.

3. Results

3.1. Climatology of Rainfall

Over the study region, the long rain season accounts for $\sim 50\%$ of the annual rainfall while the short rains account for $\sim 38\%$ (Figure 1b). The HAD region has witnessed considerable interannual variability in both seasons, as observed in the 37 years of the MSWEP v2.8 data (Figures 1c and 1d). A change point detection analysis reveals the existence of distinct change points for the long rains in 1998, and for the short rains in 2001. The anomalously dry long rains post-1998 reported by other studies are distinctly visible in the study region, while some recovery is seen in the later years, although subjected to high interannual variability. These results are in agreement with recent studies which identified distinct wet (1980–1997), dry (1999–2011), and recovery (from 2012 onwards) periods (Wainwright et al., 2019; Walker et al., 2020). The mean reduction in the long rains after

the change point is ~ 45 mm, that is, a decrease of $\sim 26\%$ compared to the mean rainfall over 1980–1997). In contrast to the long rains, the short rains become more abundant after the 2001 change point, albeit to a smaller extent. The mean increase in rainfall between the dry (1980–2000) and wet (2002–2016) periods is ~ 36 mm, that is, an increase of $\sim 40\%$ compared to the mean over the previous years. From 1998 to 2012, all the months during the long rains are dry, except for April in 2002 and 2006. Similarly, the anomalies in short rains are driven by uniform increases and decreases in rainfall during all its constituent months, with few exceptions. We clearly see the impact of the unprecedented El Niño event in 1997 (McPhaden, 1999) on all 3 months of the short rains, and to a lesser extent in 2006 and 2015 (which have been documented as years of high groundwater recharge (Adloff et al., 2022)), and during the exceptional drought of 2010.

3.2. Climatology of Source Regions

The climatological moisture source regions for the long and short rains are presented in Figure 2. To better understand the role of circulation patterns in influencing rainfall over the region, long-term mean integrated water vapor transport (IVT) maps for the two seasons are plotted (Figure 2) using ERA-Interim data. During the long rains, the role of the Indian Ocean as the predominant moisture source for the HAD region is evident (Figure 2a). The source region consists of two distinct lobes in the Indian Ocean, one in the northern Indian Ocean (hereafter referred to as “NIO”) and one in the southern Indian Ocean (hereafter referred to as “SIO”). While the NIO lobe stretches to the Arabian Sea on the western coast of the Indian peninsula, the SIO lobe encompasses a much larger area. The NIO and SIO lobes converge close to the HAD region. Although the source region spans a large area, half the rainfall during the long rains is estimated to originate from oceanic regions in close proximity to the HAD (red contour in Figure 2a). From the mean IVT map for the long rains (Figure 2c), it is evident that the SIO region, the largest source of moisture for HAD rainfall, is part of a large band of moisture which stretches across the tropics. We see that much of the moisture is transported to the southern parts of the HAD. The air above the NIO is relatively dry, which coincides with the existence of a persistent anticyclonic circulation pattern in the Arabian Sea (2c).

Additionally, we track the spatial dynamics of the long rains source regions and the corresponding wind patterns for the months of March, April, and May (Figures 3a–3c). We see that the moisture for the long rains is initially sourced from evaporation in the NIO in March. From the wind circulation patterns, it is clear that the lack of moisture contribution from the SIO coincides with the lack of winds from the region. As the long rain season progresses, the regions of the most intense moisture contributions gradually shift to the SIO during April and May (Figures 3b and 3c). As the contribution of March rainfall to the total rainfall is the lowest among the 3 months (Figure 1b), moisture from the SIO forms the major source during the long rains (Figure 2a).

The source region of rainfall during the short rains has a spatial pattern similar to that of the long rains, with two distinct lobes in the Northern and Southern Hemispheres (Figure 2b), and a relatively small proximate region contributing 50% of the rainfall (red contour in Figure 2b). Although the total rainfall during the short rains is less than during the long rains, the extent of the source region is larger, with the NIO lobe reaching as far as the Indian subcontinent. The change in the wind circulation patterns between the long and short rains is evident (Figure 2d), resulting in higher moisture transport from the NIO region. Temporally, the progression of the source regions through the months of October, November, and December is similar to that of the long rains, with the main difference being that the rains are initiated by moisture transport from the SIO lobe rather than the NIO region (compare Figure 3d with Figure 3a). In the subsequent months (November and December), the regions contributing the largest amount of evaporation are in the Northern Hemisphere (Figures 3e and 3f). Unlike the long rains, the NIO and SIO are equally important as source regions for rainfall. Finally, as for the long rains, higher moisture contributions from the NIO and SIO are generally associated with favorable circulation conditions and stronger winds.

To quantify the relative importance of different regions for rainfall over the HAD, we differentiate between three distinct source regions: (a) *local land*, that is, any land areas within the HAD region, (b) *ocean*, and (c) *external land*, that is, any land areas outside the HAD region. The contribution from local land evaporation to HAD precipitation is defined as the *local recycling*. Table 1 shows the percentage of total rainfall that originates from each of the three regions. The dominant role of the ocean as a source of moisture for rainfall during the long and short rains is reflected in the relative contributions, in which evaporation from the oceans contributes more than 75% of the total moisture. In terms of local land contributions, local recycling of moisture plays a greater role

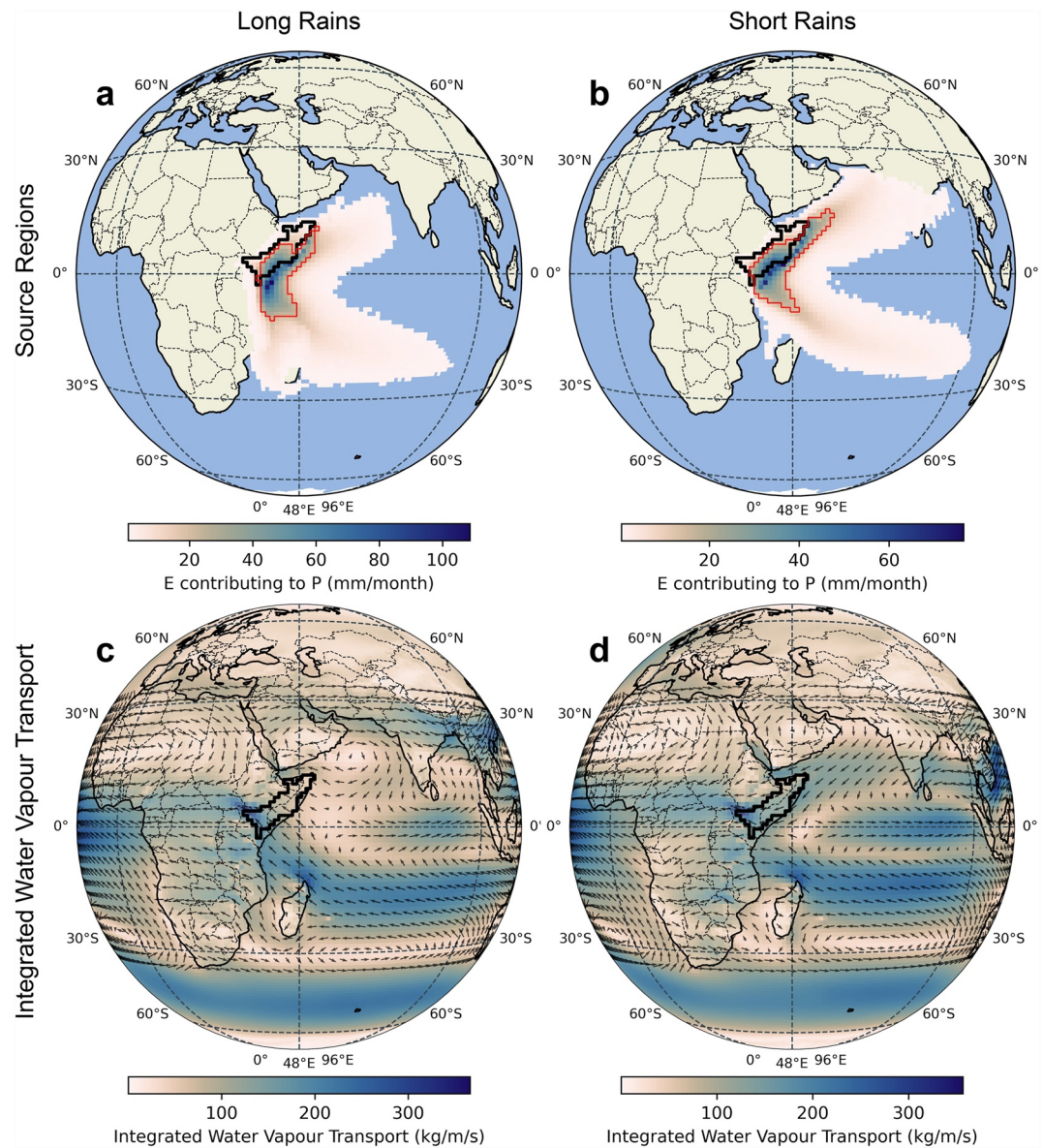


Figure 2. (a) and (b) Source regions of rainfall during long (a) and short (b) rains, averaged over the time period 1980–2016. The source region represents the smallest region contributing 95% of the climatological mean rainfall during the long and short rains. The red outline corresponds to the smallest source region contributing 50% of the rainfall for each season. c and (d) Long-term mean in integrated water vapor transport (IVT) during the long (c) and short (d) rains. The arrows represent the corresponding prevailing wind directions.

during the short rains compared to the long rains. Decomposing the relative contributions into the constituent months, we see that the land contributions (both external and local recycling) are the lowest during the first month of both seasons (March for the long rains and October for the short rains). The land contributions peak during the second month of both seasons, with as much as 28% of the short rains coming from land evaporation (local recycling plus external land contributions) in November (see Table 1).

3.3. Trends and Multi-Annual Variability in Sources

While the previous section focused on quantifying the climatological mean source regions of both the long and short rains, here we quantify the temporal changes in the moisture contributions of the three source regions (defined above) to the total rainfall during both seasons. This is especially important given the large year-to-year

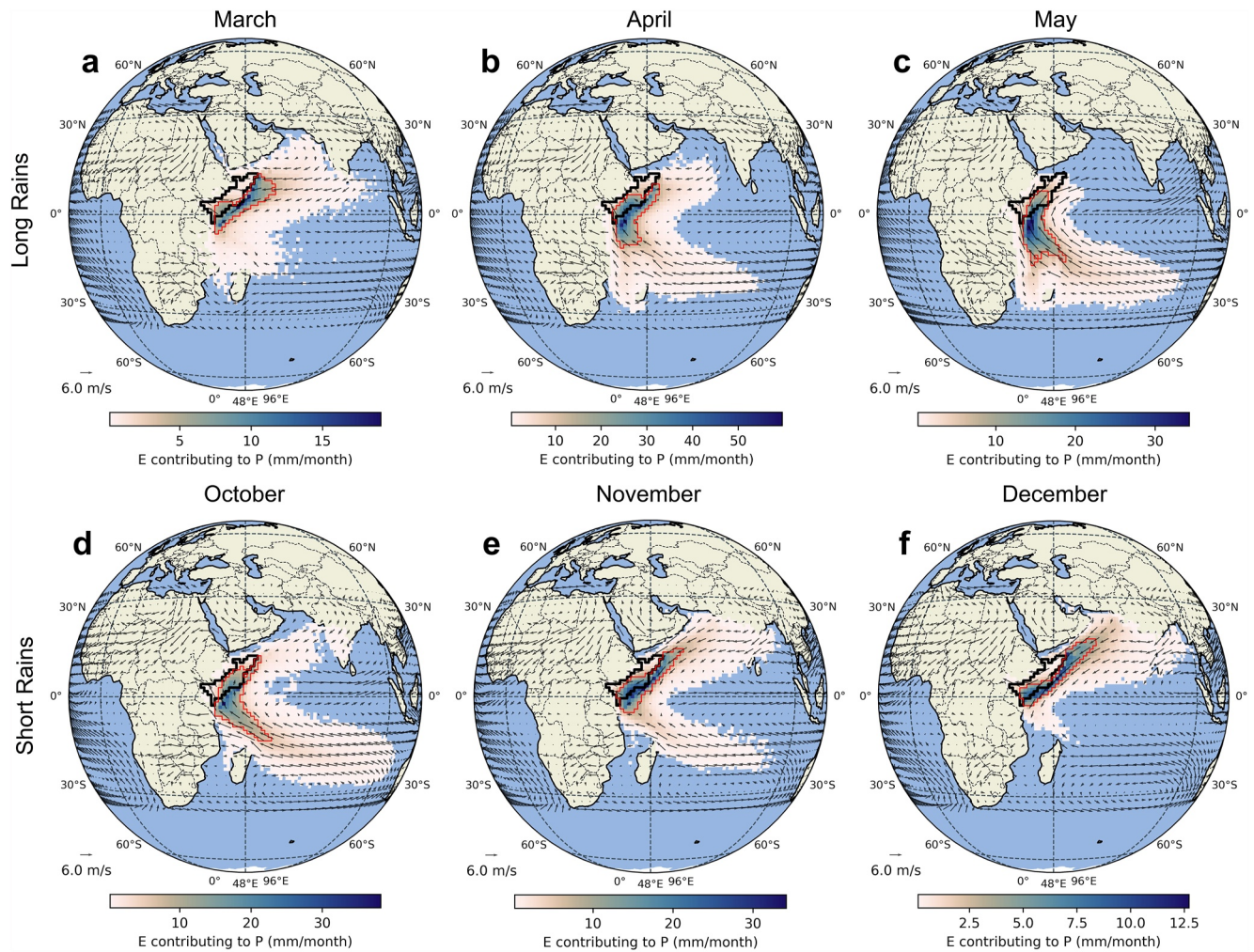


Figure 3. Source regions of rainfall for March (a), April (b), May (c), October (d), November (e), and December (f), calculated over the time period 1980–2016. The arrows represent wind magnitude and direction at 850 hPa.

variability in rainfall that impacts the HAD region (Adloff et al., 2022). Further, we identify the regions from which moisture contribution is enhanced/inhibited during anomalously wet and dry years. From Figure 4a, we see that the moisture contributions from all three source regions are closely correlated with total rainfall: both land and ocean contributions concurrently increase or decrease with total rainfall. A few exceptions exist (years 1983, 1998, 2002, 2003, and 2005), wherein land contributions were anomalously negative while ocean contributions were positive (note that anomalies are not shown in the figure). To quantify this apparent association among the three sources, we estimate the pairwise correlation among them. We see that the two land sources

Table 1
Percentage Contribution (Mean) and the Associated Standard Deviation of Different Source Regions to Rainfall Over the HAD Region

Source	Long rains	Short rains	March	April	May	October	November	December
Local recycling	10.9 ± 3.1	13.8 ± 4.3	7.1 ± 5.4	15.0 ± 4.9	10.7 ± 3.0	11.9 ± 3.9	17.3 ± 5.2	12.2 ± 6.3
Ocean	78.6 ± 5.0	76.7 ± 5.3	84.5 ± 8.2	73.4 ± 7.3	77.9 ± 5.9	80.7 ± 5.4	72.0 ± 6.1	77.6 ± 7.5
External land	10.5 ± 2.3	7.6 ± 1.3	8.4 ± 4.2	11.6 ± 2.9	11.4 ± 3.8	7.4 ± 1.9	10.7 ± 1.5	10.2 ± 2.2

Note. The mean and standard deviation values are computed from monthly and seasonal mean estimates of moisture contribution calculated for the time period 1980–2016.

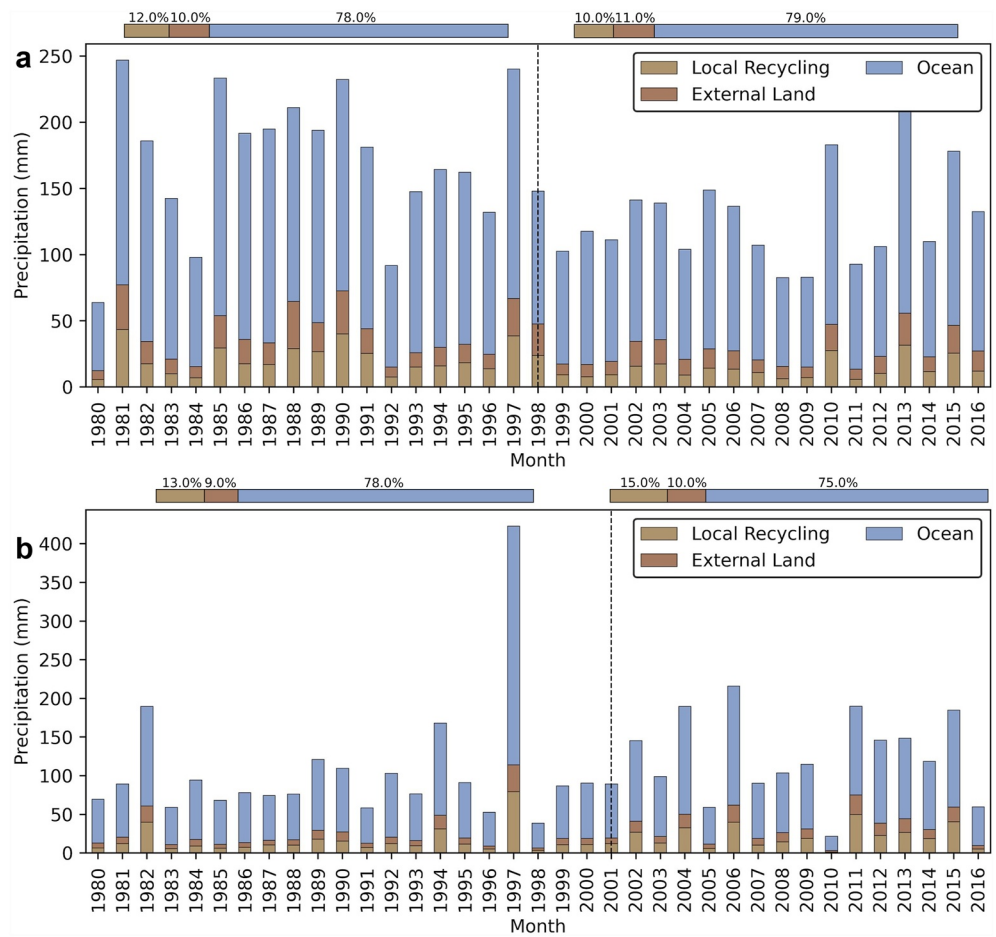


Figure 4. Time series of moisture contributions to rainfall from local recycling, external land, and ocean sources during the long (a) and short (b) rains, respectively. The horizontal bars at the top of the plots represent the relative percentage contribution from different sources before and after the change point.

(local and external land) have the highest correlation (0.94), followed by ocean contributions and local recycling (0.84), and, finally, ocean contributions and external land (0.79). Further, we estimate the difference in relative moisture contributions from the three sources before and after the change point in 1998. The absolute moisture contribution from the oceans, the largest (Table 1), has witnessed a reduction of $\sim 25\%$ (-33.8 mm) compared to the pre-change point period; while the relative importance of oceanic moisture remains similar. Simultaneously, locally recycled moisture has decreased by $\sim 33\%$ (-6.8 mm) and from 12% to 10% after 1998. Finally, the moisture contributions from external land surfaces experienced a change of $\sim -23\%$ (-4.3 mm).

Similar to the long rains, we see that the moisture contributions from each of the source regions during the short rains are strongly correlated with each other (Figure 4b). We do not see any year in which land sources have alleviated moisture deficits from the ocean, that is, anomalously enhanced or inhibited moisture contribution from the ocean is also associated with enhanced or inhibited moisture contribution from the land, respectively (Figure 4b). Next, we analyze the changing moisture contribution from the different sources before and after the change point in 2001. While the absolute ocean contribution has seen an increase of $\sim 31\%$ (21.6 mm) along with an increase in the total rainfall after the break point, the relative importance of ocean evaporation for rainfall during the short rains has been decreasing (from 78% to 75%). Meanwhile, the land contributions have witnessed a remarkable change with the locally recycled moisture and external land contributions increasing by $\sim 80\%$ (9.7 mm) and $\sim 59\%$ (4.9 mm).

3.4. Source Regions During dry and Wet Years

To better understand the variability of the source regions during extreme rainfall, we first average the source regions of the five wettest (1981, 1985, 1987, 1988, 1990) and driest (1999, 2004, 2008, 2009, 2011) years of

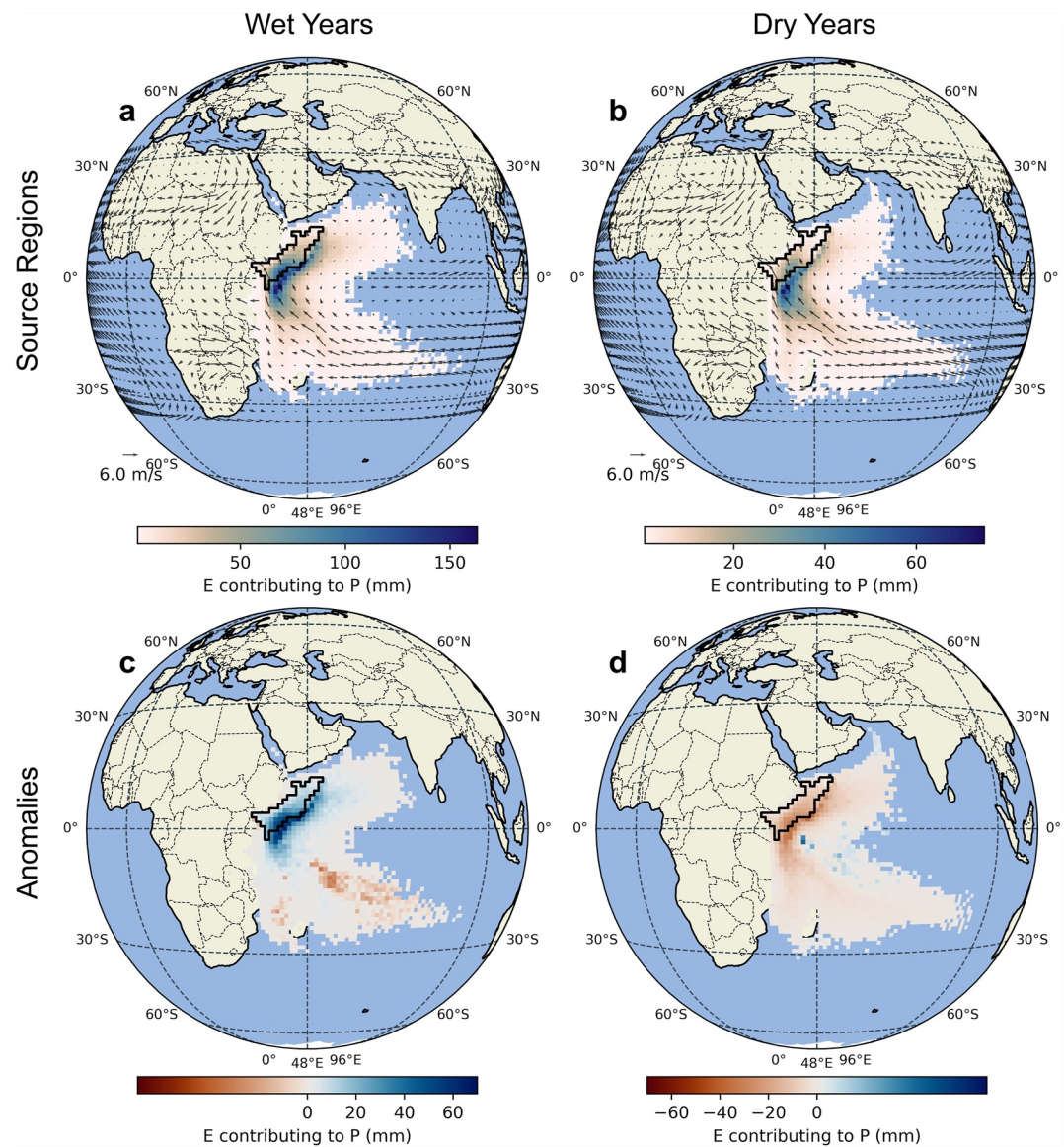


Figure 5. (a) and (b) Source regions of rainfall over the Horn of Africa drylands during the long rains, averaged over anomalously wet (a) and dry (b) years, respectively. The arrows represent wind speed and direction at 850 hPa. (c) and (d) Anomalies of source region contributions to rainfall for the cases shown in (a) and (b), respectively.

the long rains (Figures 5a and 5b). The spatial extent of moisture-contributing regions is similar between wet and dry years, with the main difference being the absolute magnitude of the moisture contribution from the source regions. To better understand the magnitude by which moisture contribution to rainfall is enhanced or inhibited in the source regions, we calculate the anomalies of source region contributions for the wet and dry years (Figures 5c and 5d). The higher rainfall during the wet years can be attributed to enhanced moisture contributions from relatively small areas in close proximity to the HAD region. In fact, the contribution from a substantial part of the *SIO* is anomalously low. In contrast, the reduced rainfall in dry years is a result of severely inhibited moisture contribution from most of the source region, with only a small area in the *SIO* exhibiting near-zero or positive anomalies. Interestingly, the difference in wind speed between wet and dry years is negligible.

We perform a similar analysis for the short rains by averaging the source regions of the five wettest (1982, 2004, 2006, 2011, and 2015) and driest (1983, 1991, 1998, 2005, and 2010) years (Figures 6a and 6b), respectively, and estimate their anomalies (Figures 6d and 6e). The wet years are typically associated with positive ENSO and IOD; the seasonal mean of the multivariate ENSO index (<https://www.psl.noaa.gov/enso/mei/>) and the Dipole

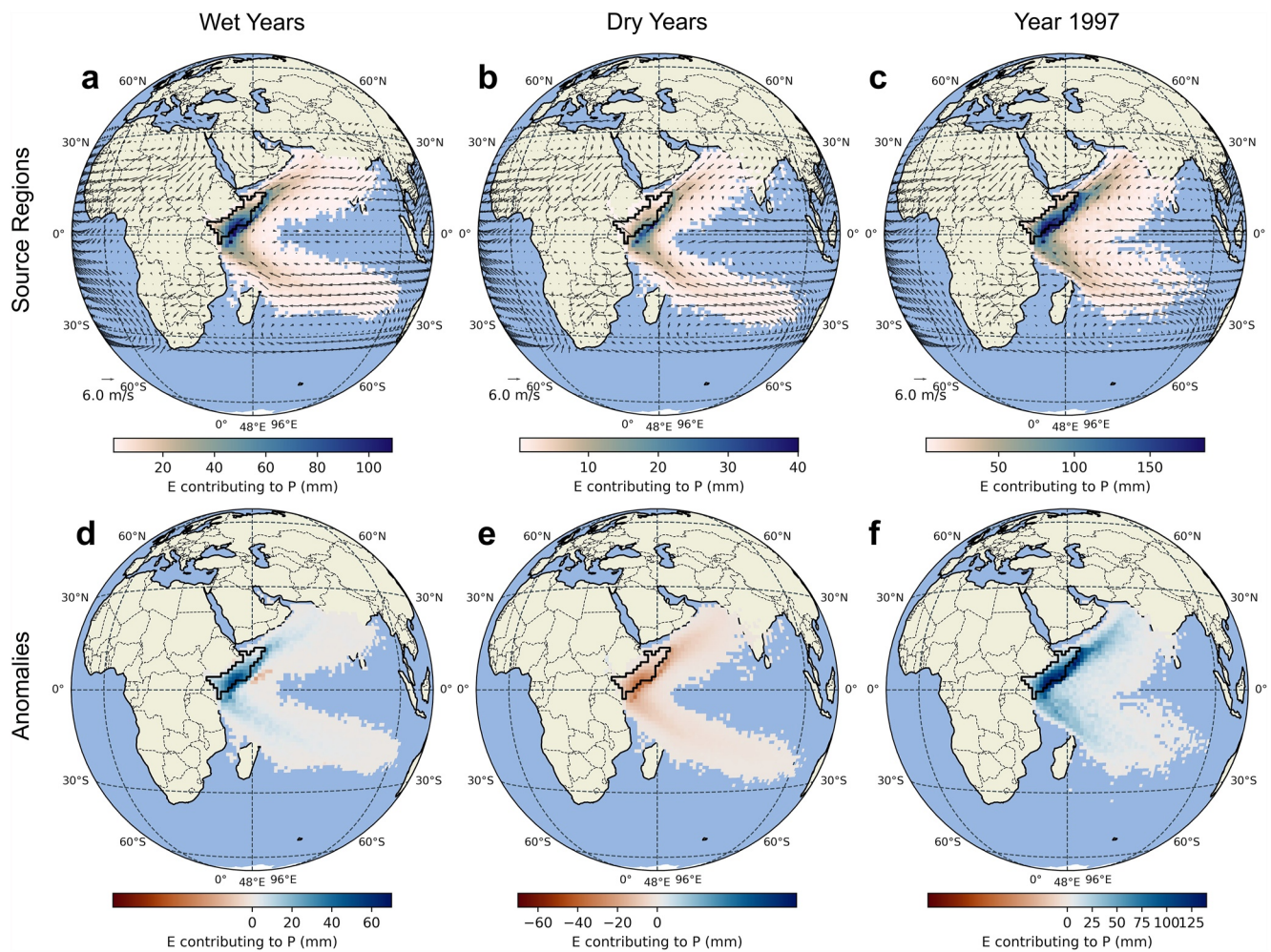


Figure 6. (a), (b), and (c) Source regions of evaporation contributing to rainfall over the Horn of Africa drylands during the short rains, averaged over anomalously wet (a), dry (b) years and the exceptional El Niño and IOD year of 1997 (c), respectively. Arrows represent wind speed and direction at 850 hPa. (d), (e), and (f) Anomalies of evaporation from the source region for the cases shown in (a), (b), and (c), respectively.

Mode Index (https://psl.noaa.gov/gcos_wgsp/Timeseries/DMI/) over the 5 years were +1.1 and +0.35, respectively. The dry-year seasonal mean of the multivariate ENSO index and the Dipole Mode Index were -0.64 and -0.18 , respectively. Unlike the long rains, we see a tangible increase in the area of the source regions contributing moisture during the wet years compared to the dry years (compare Figures 6a and 6b), with even land areas in the Indian subcontinent contributing to rainfall. In addition, moisture contributions from most of the source regions are anomalously positive (Figure 6d), in contrast to the long rains in which enhanced moisture contributions were only seen from regions proximate to the HAD (Figure 5c). Similarly, the anomalies for the dry years indicate that moisture contribution is inhibited from the entire source region. As the short rains are closely associated with ENSO and IOD (MacLeod et al., 2021), the expansion and contraction of the source regions are likely related to the strength of these oscillations.

An extreme case of the ENSO and IOD influence is seen in 1997 (McPhaden, 1999). The multivariate ENSO index was at an unprecedented value of +2.0 and the Dipole Mode index was recorded at a historically high value of +1.2. We see that the record high rainfall of approximately 300 mm averaged over the HAD region originated from a much larger source region than normal (Figure 6c), with an expansion of both *NIO* and *SIO* lobes. Additionally, anomalies of ocean moisture contribution were exceedingly positive over the entire source region, with magnitudes doubling that of even the other wet years (compare Figures 6d and 6f). Similar to the long rains, we observe no significant changes in either the average wind direction or associated circulation patterns across the wet, dry, or ENSO-dominated years. However, we do notice stronger westerlies across the equatorial Indian

Ocean. On the contrary, wind speeds are marginally higher during the dry years, despite the lower moisture contributions. However, we see that winds diverge away from the HAD region in the *NIO* lobe, reducing the amount of moisture being transported from far away to the region.

4. Discussion

4.1. Indian Ocean as the Dominant Source of Moisture for HAD Rainfall

The results of this study re-emphasize the dominant role of the Indian Ocean as a moisture source for the long and short rains in the HAD region (C. C. Funk et al., 2016; Wainwright et al., 2019; Walker et al., 2020; Williams & Funk, 2011). In fact, on a global average, oceanic moisture sources are likely becoming more important for continental rainfall as a result of climate change (Findell et al., 2019; Gimeno et al., 2020). Therefore, a key step in improving the current understanding of the intraseasonal and interannual variability of the two rain seasons in HAD is to accurately characterize the variability in moisture source regions within the Indian Ocean. In this regard, our results agree with previous global-scale studies; based on ERA-Interim reanalysis as well, Van der Ent and Savenije (2013) and Nieto et al. (2014) delineated source regions of continental precipitation that agree with the *NIO* and *SIO* lobes in Figure 2. These two regions are among the 15 major oceanic sources of terrestrial rainfall identified by Van der Ent and Savenije (2013), and similar sources were also portrayed by Gimeno et al. (2010). Further, the evolution of the predominant source regions—from (a) *NIO* to the *SIO* through the months of March, April, May during the long rains and (b) from *SIO* to the *NIO* over the course of the 3 months (OND) during the short rains—seen in Figure 3—matches the findings of Van der Ent and Savenije (2013) and MacLeod (2019). The *NIO* region (2) is consistent with the circulation patterns associated with the north-east monsoon during which moisture-laden winds blow from the Western Ghats mountain range in India toward Somalia (November, December, and March in Figure 3) (C. C. Funk et al., 2016). On the other hand, the *SIO* moisture source region encompasses regions influenced by the Somali low-level jet, a well-known conveyor of moisture to East Africa during the months of April, May, and October (Figure 3) (Munday et al., 2021).

Figures 5 and 6 show that variability in rainfall over the HAD region is strongly driven by the near-uniform inhibition/enhancement of moisture contribution from all oceanic source regions. However, delineating source regions and their moisture contributions alone is insufficient to fully understand the primary reasons for changes in moisture contributions. To address this, we compare the precipitation over the HAD region with the total evaporation (as opposed to moisture contributions to rainfall) from the source regions for the long and short rains (Figure 7). From Figure 7, it is clear that long rain precipitation and evaporation in the source region are, in fact, anti-correlated (correlation coefficient of -0.52). Similarly, the short rains exhibit a negative correlation with source region evaporation, albeit with a lower correlation coefficient of -0.15 . This indicates that changes in the long and short rains are not primarily controlled by changes in ocean evaporation in source regions. From this, we infer that rainfall changes must be driven instead by atmospheric circulation and dynamic and thermodynamic processes determining atmospheric stability in the sink region.

4.2. The Importance of Terrestrial Evaporation for HAD Rainfall

While the contribution of terrestrial moisture sources to rainfall in the HAD region is low, it is nevertheless substantial, with 20%–25% of the rainfall originating over land. In an arid region like the HAD, land contributions can be the difference between a drought and an average rainfall season (Miralles et al., 2016). However, this does not imply that the land contributions can alleviate the reduced moisture contribution from oceans during the dry years. As evident from our results, ocean and land contributions are closely correlated with each other. During the long rains, the contribution from land generally increases if contributions from the ocean to rainfall over HAD increase too (the correlation between ocean contributions and locally recycled moisture is 0.84; external land and ocean contributions exhibit a correlation of 0.79). This may partly be due to the fact that the dry season water availability over land in the HAD is very low (Figure 1b) and thus most of the water available for evaporation, and the subsequent recycling, is dependent on the quantity of rainfall during the first month of the long rain season. This hypothesis is supported by increased local contributions during the second month of the rain season. Similarly, during the short rains, the correlations between ocean contribution and locally recycled and external land contributions are 0.93 and 0.98, respectively. There exists a strong association of the short rains with large-scale ocean–atmosphere oscillations such as ENSO and IOD, during which land evaporation is dependent

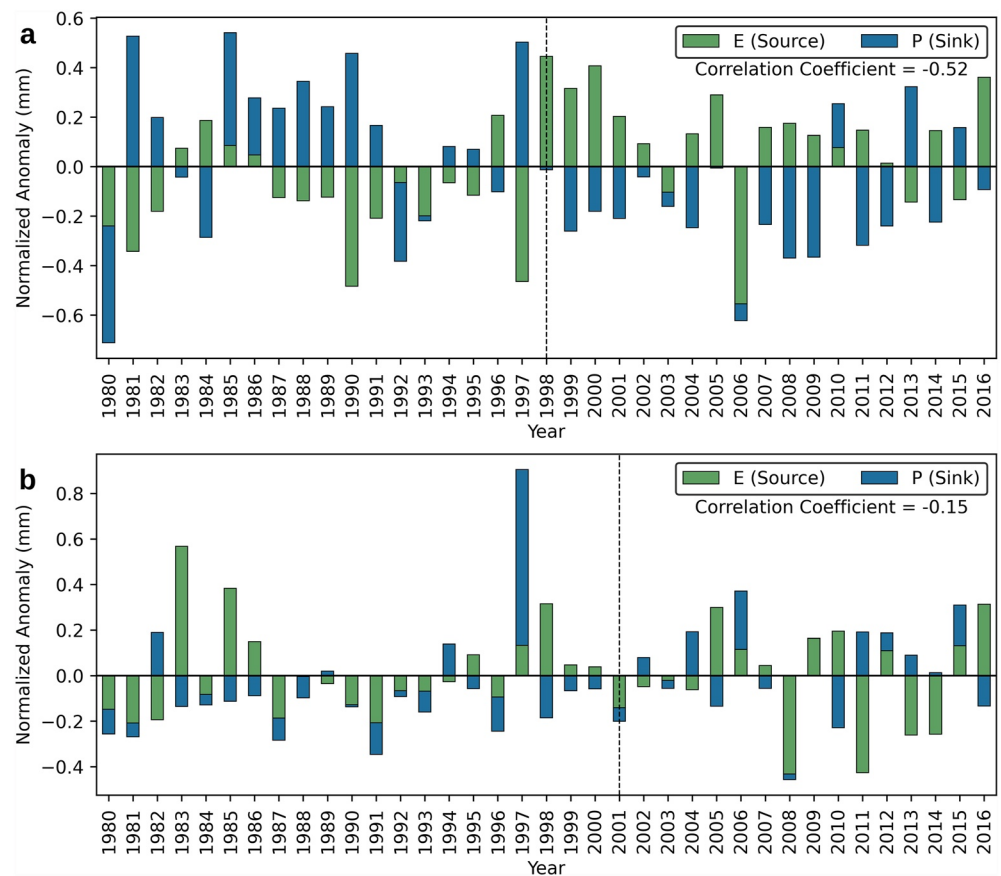


Figure 7. Time series of normalized anomalies of total evaporation from the source region (E (Source)) compared to precipitation in the HAD region (P (sink)) for the long (a) and short (b) rains. E (source) is estimated by weighing evaporation from each grid cell in the source region by their relative contribution to rainfall in the HAD region.

on the quantity of rainfall in the first month of the short rains (October). This has implications for the evolution of droughts in the HAD region: lower ocean-driven moisture contribution to rainfall during the first month of the rainy season could trigger exacerbated drought conditions in the subsequent months due to progressive reduction in moisture contribution from land surfaces. Although land contributions to rainfall are relatively low, substantial changes in their magnitude could make the difference between a normal and a below-normal rainfall season.

We contextualize the importance of land contributions in the HAD region by comparing them with those of different regions across Africa. In contrast to the dominant role of the Indian Ocean reported above, the Sahel region in Sudan derives the majority of moisture for its rainfall (~60%) from terrestrial sources (Salih et al., 2015). Similarly, land-derived moisture contributions account for ~60% and ~44% of the rainfall over the Congo rainforest (Tuinenburg et al., 2020) and West Africa (Gong & Eltahir, 1996), respectively. Continental-scale studies have shown that ~50% of the rainfall over Africa is derived from terrestrial sources (Te Wierik et al., 2022; van der Ent et al., 2010). However, there exists some spatial variability; for example, in the Limpopo river basin in southern Africa (Rapolaki et al., 2020) which is closer to the oceans compared to the Sahel, the moisture sources are predominantly oceanic. However, proximity to the oceans does not necessarily imply greater moisture contribution from them (examples include the Yangtze River valley in Asia (Fremme & Sodemann, 2019) and the western coast of Africa (van der Ent et al., 2010)). The local recycling results reported in this study (Table 1) are in line with a global analysis of water-limited regions which showed that local recycling can contribute 3%–35% of the rainfall in dry regions (Miralles et al., 2016).

5. Conclusion

Rainfall in the HAD region is influenced by a complex set of factors including large-scale circulation patterns and oscillations combined with local dynamical and thermodynamic factors. Therefore, deriving new insights

into the drivers of the HAD rainfall at multiple timescales is essential for improving its predictability. To this end, the study addressed two major research objectives: (a) to understand and quantify the relative contributions of different sources of rainfall to the trends in rainfall during two major rainfall seasons in the HAD region and (b) to quantify the role of the land in influencing HAD seasonal rainfall during and wet and dry periods.

In addressing these objectives, the study mapped the main sources of moisture associated with the north-east monsoon and the Somali low-level jet, the two main atmospheric circulation patterns which transport moisture to the HAD region. Specifically, ocean contributions amount to ~80% of the HAD rainfall. Our results reveal that while land contributions, which amount to ~20% of the HAD rainfall, are becoming increasingly important for the short rains in recent years, the importance of ocean contributions is increasing for the long rains. The relatively small but substantial moisture contribution from land during the two rain seasons highlights the importance of vegetation transpiration, interception loss, and soil evaporation as sources of rainfall. Further, our results highlight the complex combination of drivers (changes in source region evaporation, regional circulation patterns, and local atmospheric stability) that potentially drive the variability in long rains. Specifically, we find that during the long rains evaporation from the source region is anti-correlated with rainfall in the HAD. Unraveling the mechanisms behind this strong anti-correlation can provide insights into the decline of the long rains and thus the *East African paradox*.

At seasonal and subseasonal scales, the source regions derived with the Lagrangian analysis have the potential to improve the predictability of the long and short rains through both better selection of predictors (Demam et al., 2022) and improving the understanding of their drivers. Therefore, our results can be used to augment drought and flood early warning systems, which are important tools in the region to prepare appropriate mitigation measures (C. Funk et al., 2019). At interannual timescales, the Lagrangian perspective provided in this study can help disentangle the complex drivers of the two rain seasons, especially the more elusive drivers of the long rains. At decadal time scales, the source regions enable novel ways of evaluating the current generation of climate models, which still exhibit a high degree of uncertainty and disagreement in simulating rainfall over the region.

Data Availability Statement

The data required for reproducing the results and figures in the main text have been deposited in <https://doi.org/10.5281/zenodo.7452390> (Koppa et al., 2022). The codes required for reproducing the results and figures in this study are available at <https://doi.org/10.5281/zenodo.7452372> (Koppa, 2022).

Acknowledgments

The study was funded by the European Union Horizon 2020 Programme (DOWN2EARTH, 869.550). J.K. is grateful for the support from the Research Foundation–Flanders (FWO) under Grant 1244122N. The computational resources and services used in this work were provided by the VSC (Flemish Supercomputer Center), funded by the Research Foundation, Flanders (FWO), and the Flemish Government. A.K., J.K., and D.G.M conceived the study and designed the experiments. A.K. conducted the analysis with inputs from J.K., D.A.M., and D.G.M. A.K. wrote the paper with contributions from all coauthors. All coauthors contributed to the interpretation and discussion of results.

References

- Adloff, M., Singer, M. B., MacLeod, D. A., Michaelides, K., Mehrnegar, N., Hansford, E., et al. (2022). Sustained water storage in horn of Africa drylands dominated by seasonal rainfall extremes. *Geophysical Research Letters*, *49*(21), e2022GL099299. <https://doi.org/10.1029/2022GL099299>
- Beck, H. E., Wood, E. F., Pan, M., Fisher, C. K., Miralles, D. G., Van Dijk, A. I. J. M., et al. (2019). Msweb v2 global 3-hourly 0.1° precipitation: Methodology and quantitative assessment. *Bulletin of the American Meteorological Society*, *100*(3), 473–500. <https://doi.org/10.1175/BAMS-D-17-0138.1>
- Behera, S. K., Luo, J.-J., Masson, S., Delecluse, P., Gualdi, S., Navarra, A., & Yamagata, T. (2005). Paramount impact of the Indian Ocean Dipole on the East African short rains: A CGCM study. *Journal of Climate*, *18*(21), 4514–4530. <https://doi.org/10.1175/JCLI3541.1>
- Brown, M. E., & Funk, C. C. (2008). Food security under climate change. *Science*, *319*(5863), 580–581. <https://doi.org/10.1126/science.1154102>
- Dee, D. P., Uppala, S. M., Simmons, A. J., Berrisford, P., Poli, P., Kobayashi, S., et al. (2011). The era-interim reanalysis: Configuration and performance of the data assimilation system. *Quarterly Journal of the Royal Meteorological Society*, *137*(656), 553–597. <https://doi.org/10.1002/qj.828>
- Demam, V. M. H., Koppa, A., Waegeman, W., MacLeod, D. A., Bliss Singer, M., & Miralles, D. G. (2022). Seasonal prediction of horn of Africa long rains using machine learning: The pitfalls of preselecting correlated predictors. *Frontiers in Water*, *4*. <https://doi.org/10.3389/frwa.2022.1053020>
- Drumond, A., Nieto, R., Gimeno, L., & Ambrizzi, T. (2008). A Lagrangian identification of major sources of moisture over central Brazil and La Plata basin. *Journal of Geophysical Research*, *113*(D14), D14128. <https://doi.org/10.1029/2007JD009547>
- Dyer, E., & Washington, R. (2021). Kenyan long rains: A subseasonal approach to process-based diagnostics. *Journal of Climate*, *34*(9), 3311–3326. <https://doi.org/10.1175/JCLI-D-19-0914.1>
- Dyer, E. L. E., Jones, D. B. A., Nusbaumer, J., Li, H., Collins, O., Vettoretti, G., & Noone, D. (2017). Congo basin precipitation: Assessing seasonality, regional interactions, and sources of moisture. *Journal of Geophysical Research: Atmospheres*, *122*(13), 6882–6898. <https://doi.org/10.1002/2016JD026240>
- Emanuel, K. A. (1991). A scheme for representing cumulus convection in large-scale models. *Journal of the Atmospheric Sciences*, *48*(21), 2313–2329. [https://doi.org/10.1175/1520-0469\(1991\)048<2313:asfrec>2.0.co;2](https://doi.org/10.1175/1520-0469(1991)048<2313:asfrec>2.0.co;2)
- Fewsnet. (2022). Immediate global action required to prevent famine in the horn of Africa. Retrieved from https://fews.net/sites/default/files/Joint%20Alert%20on%202023%20MAM%20Rains%20Final_0.pdf

- Findell, K. L., Keys, P. W., Van der Ent, R. J., Lintner, B. R., Berg, A., & Krasting, J. P. (2019). Rising temperatures increase importance of oceanic evaporation as a source for continental precipitation. *Journal of Climate*, 32(22), 7713–7726. <https://doi.org/10.1175/JCLI-D-19-0145.1>
- Fremme, A., & Sodemann, H. (2019). The role of land and ocean evaporation on the variability of precipitation in the yangtze river valley. *Hydrology and Earth System Sciences*, 23(6), 2525–2540. <https://doi.org/10.5194/hess-23-2525-2019>
- Funk, C., Harrison, L., Shukla, S., Pomposi, C., Galu, G., Korecha, D., et al. (2018). Examining the role of unusually warm indo-pacific sea-surface temperatures in recent African droughts. *Quarterly Journal of the Royal Meteorological Society*, 144(S1), 360–383. <https://doi.org/10.1002/qj.3266>
- Funk, C., Shukla, S., Thiaw, W. M., Rowland, J., Hoell, A., McNally, A., et al. (2019). Recognizing the famine early warning systems network: Over 30 years of drought early warning science advances and partnerships promoting global food security. *Bulletin of the American Meteorological Society*, 100(6), 1011–1027. <https://doi.org/10.1175/BAMS-D-17-0233.1>
- Funk, C. C., Hoell, A., Shukla, S., Husak, G. J., & Michaelsen, J. (2016). The east African monsoon system: Seasonal climatologies and recent variations: Chapter 10. In *The monsoons and climate change* (pp. 163–185). Springer. https://doi.org/10.1007/978-3-319-21650-8_8
- García-Herrera, R., Garrido-Perez, J. M., Barriopedro, D., Ordóñez, C., Vicente-Serrano, S. M., Nieto, R., et al. (2019). The European 2016/17 drought. *Journal of Climate*, 32(11), 3169–3187. <https://doi.org/10.1175/JCLI-D-18-0331.1>
- Gimeno, L., Drumond, A., Nieto, R., Trigo, R. M., & Stohl, A. (2010). On the origin of continental precipitation. *Geophysical Research Letters*, 37(13). <https://doi.org/10.1029/2010gl043712>
- Gimeno, L., Nieto, R., & Sorí, R. (2020). The growing importance of oceanic moisture sources for continental precipitation. *npj Climate and Atmospheric Science*, 3(1), 27. <https://doi.org/10.1038/s41612-020-00133-y>
- Gong, C., & Eltahir, E. (1996). Sources of moisture for rainfall in west Africa. *Water Resources Research*, 32(10), 3115–3121. <https://doi.org/10.1029/96wr01940>
- Haile, G. G., Tang, Q., Hosseini-Moghari, S.-M., Liu, X., Gebremicael, T. G., Leng, G., et al. (2020). Projected impacts of climate change on drought patterns over east Africa. *Earth's Future*, 8(7), e2020EF001502. <https://doi.org/10.1029/2020ef001502>
- Herrera-Estrada, J. E., Martínez, J. A., Domínguez, F., Findell, K. L., Wood, E. F., & Sheffield, J. (2019). Reduced moisture transport linked to drought propagation across North America. *Geophysical Research Letters*, 46(10), 5243–5253. <https://doi.org/10.1029/2019GL082475>
- Hersbach, H., Bell, B., Berrisford, P., Hirahara, S., Horányi, A., Muñoz-Sabater, J., et al. (2020). The era5 global reanalysis. *Quarterly Journal of the Royal Meteorological Society*, 146(730), 1999–2049. <https://doi.org/10.1002/qj.3803>
- Holgate, C. M., Van Dijk, A. I. J. M., Evans, J. P., & Pitman, A. J. (2020). Local and remote drivers of southeast Australian drought. *Geophysical Research Letters*, 47(18), e2020GL090238. <https://doi.org/10.1029/2020gl090238>
- Hsiang, S. M., Burke, M., & Miguel, E. (2013). Quantifying the influence of climate on human conflict. *Science*, 341(6151), 1235367. <https://doi.org/10.1126/science.1235367>
- Huffman, G. J., Bolvin, D. T., Braithwaite, D., Hsu, K., Joyce, R., Xie, P., & Yoo, S.-H. (2015). Nasa global precipitation measurement (gpm) integrated multi-satellite retrievals for gpm (imerg). *Algorithm Theoretical Basis Document (ATBD) Version*, 4(26).
- Keune, J., & Miralles, D. G. (2019). A precipitation recycling network to assess freshwater vulnerability: Challenging the watershed convention. *Water Resources Research*, 55(11), 9947–9961. <https://doi.org/10.1029/2019wr025310>
- Keune, J., Schumacher, D. L., & Miralles, D. G. (2022). A unified framework to estimate the origins of atmospheric moisture and heat using Lagrangian models. *Geoscientific Model Development*, 15(5), 1875–1898. <https://doi.org/10.5194/gmd-15-1875-2022>
- Koppa, A. (2022). A Lagrangian analysis of the sources of rainfall over the horn of Africa drylands (version 1.0.0.) [Software]. Zenodo. <https://doi.org/10.5281/zenodo.7452372>
- Koppa, A., Keune, J., & Diego, D. G. (2022). A Lagrangian analysis of the sources of rainfall over the horn of Africa drylands (version 1.0.0.) [Dataset]. Zenodos. <https://doi.org/10.5281/zenodo.7452390>
- Liebmann, B., Hoerling, M. P., Funk, C., Bladé, I., Dole, R. M., Allured, D., et al. (2014). Understanding recent eastern horn of Africa rainfall variability and change. *Journal of Climate*, 27(23), 8630–8645. <https://doi.org/10.1175/jcli-d-13-00714.1>
- MacLeod, D. (2019). Seasonal forecasts of the East African long rains: Insight from atmospheric relaxation experiments. *Climate Dynamics*, 53(7), 4505–4520. <https://doi.org/10.1007/s00382-019-04800-6>
- MacLeod, D., Graham, R., O'Reilly, C., Otieno, G., & Todd, M. (2021). Causal pathways linking different flavours of ENSO with the greater horn of Africa short rains. *Atmospheric Science Letters*, 22(2), e1015. <https://doi.org/10.1002/asl.1015>
- Manatsa, D., & Behera, S. K. (2013). On the epochal strengthening in the relationship between rainfall of east Africa and iod. *Journal of Climate*, 26(15), 5655–5673. <https://doi.org/10.1175/jcli-d-12-00568.1>
- Martens, B., Miralles, D. G., Lievens, H., Van der Schalie, R., De Jeu, R. A. M., Fernández-Prieto, D., et al. (2017). Glean v3: Satellite-based land evaporation and root-zone soil moisture. *Geoscientific Model Development*, 10(5), 1903–1925. <https://doi.org/10.5194/gmd-10-1903-2017>
- Maystadt, J.-F., & Ecker, O. (2014). Extreme weather and civil war: Does drought fuel conflict in Somalia through livestock price shocks? *American Journal of Agricultural Economics*, 96(4), 1157–1182. <https://doi.org/10.1093/ajae/aa010>
- McPhaden, M. J. (1999). Genesis and evolution of the 1997–98 el nino. *Science*, 283(5404), 950–954. <https://doi.org/10.1126/science.283.5404.950>
- Miralles, D. G., Holmes, T. R. H., De Jeu, R. A. M., Gash, J. H., Meesters, A. G. C. A., & Dolman, A. J. (2011). Global land-surface evaporation estimated from satellite-based observations. *Hydrology and Earth System Sciences*, 15(2), 453–469. <https://doi.org/10.5194/hess-15-453-2011>
- Miralles, D. G., Nieto, R., McDowell, N. G., Dorigo, W. A., Verhoest, N. E., Liu, Y. Y., et al. (2016). Contribution of water-limited ecoregions to their own supply of rainfall. *Environmental Research Letters*, 11(12), 124007. <https://doi.org/10.1088/1748-9326/11/12/124007>
- Munday, C., Washington, R., & Hart, N. (2021). African low-level jets and their importance for water vapor transport and rainfall. *Geophysical Research Letters*, 48(1), e2020GL090999. <https://doi.org/10.1029/2020gl090999>
- Niang, C., Mancho, A. M., García-Garrido, V. J., Mohino, E., Rodríguez-Fonseca, B., & Curbelo, J. (2020). Jul 27) Transport pathways across the west African monsoon as revealed by Lagrangian coherent structures. *Scientific Reports*, 10(1), 12543. <https://doi.org/10.1038/s41598-020-69159-9>
- Nicholson, S. E. (2015). Long-term variability of the east African ‘short rains’ and its links to large-scale factors. *International Journal of Climatology*, 35(13), 3979–3990. <https://doi.org/10.1002/joc.4259>
- Nicholson, S. E., Fink, A. H., Funk, C., Klotter, D. A., & Satheesh, A. R. (2022). Meteorological causes of the catastrophic rains of October/November 2019 in equatorial Africa. *Global and Planetary Change*, 208, 103687. <https://doi.org/10.1016/j.gloplacha.2021.103687>
- Nieto, R., Castillo, R., Drumond, A., & Gimeno, L. (2014). A catalog of moisture sources for continental climatic regions. *Water Resources Research*, 50(6), 5322–5328. <https://doi.org/10.1002/2013wr013901>
- Nieto, R., Gimeno, L., & Trigo, R. M. (2006). A Lagrangian identification of major sources of Sahel moisture. *Geophysical Research Letters*, 33(18). <https://doi.org/10.1029/2006gl027232>
- Pettitt, A. N. (1979). A non-parametric approach to the change-point problem. *Journal of the Royal Statistical Society. Series C (Applied Statistics)*, 28(2), 126–135. <https://doi.org/10.2307/2346729>

- Rapolaki, R. S., Blamey, R. C., Hermes, J. C., & Reason, C. J. C. (2020). Moisture sources associated with heavy rainfall over the limpopo river basin, southern Africa. *Climate Dynamics*, 55(5), 1473–1487. <https://doi.org/10.1007/s00382-020-05336-w>
- Rowell, D. P., Booth, B. B. B., Nicholson, S. E., & Good, P. (2015). Reconciling past and future rainfall trends over East Africa. *Journal of Climate*, 28(24), 9768–9788. <https://doi.org/10.1175/jcli-d-15-0140.1>
- Rybski, D., & Neumann, J. (2011). A review on the pettitt test pettitt-test. In J. Kropp & H.-J. Schellnhuber (Eds.), *In extremis: Disruptive events and trends in climate and hydrology* (pp. 202–213). Springer Berlin Heidelberg. https://doi.org/10.1007/978-3-642-14863-7_10
- Sahlu, D., Moges, S. A., Nikolopoulos, E. I., Anagnostou, E. N., & Hailu, D. (2017). Evaluation of high-resolution multisatellite and reanalysis rainfall products over east Africa. *Advances in Meteorology*, 2017, 1–14. <https://doi.org/10.1155/2017/4957960>
- Saji, N. H., Goswami, B. N., Vinayachandran, P. N., & Yamagata, T. (1999). A dipole mode in the tropical Indian ocean. *Nature*, 401(6751), 360–363. <https://doi.org/10.1038/43854>
- Salih, A. A. M., Zhang, Q., & Tjernström, M. (2015). Lagrangian tracing of Sahelian Sudan moisture sources. *Journal of Geophysical Research: Atmospheres*, 120(14), 6793–6808. <https://doi.org/10.1002/2015jd023238>
- Schumacher, D. L., Keune, J., Dirmeyer, P., & Miralles, D. G. (2022). Drought self-propagation in drylands due to land–atmosphere feedbacks. *Nature Geoscience*, 15(4), 262–268. <https://doi.org/10.1038/s41561-022-00912-7>
- Schumacher, D. L., Keune, J., Van Heerwaarden, C. C., Vilà-Guerau de Arellano, J., Teuling, A. J., & Miralles, D. G. (2019). Amplification of mega-heatwaves through heat torrents fuelled by upwind drought. *Nature Geoscience*, 12(9), 712–717. <https://doi.org/10.1038/s41561-019-0431-6>
- Sodemann, H. (2020). Beyond turnover time: Constraining the lifetime distribution of water vapor from simple and complex approaches. *Journal of the Atmospheric Sciences*, 77(2), 413–433. <https://doi.org/10.1175/jas-d-18-0336.1>
- Sodemann, H., Masson-Delmotte, V., Schwierz, C., Vinther, B. M., & Wernli, H. (2008). Interannual variability of Greenland winter precipitation sources: 2. Effects of north Atlantic oscillation variability on stable isotopes in precipitation. *Journal of Geophysical Research*, 113(D12), D12111. <https://doi.org/10.1029/2007jd009416>
- Sorí, R., Marengo, J. A., Nieto, R., Drumond, A., & Gimeno, L. (2018). The atmospheric branch of the hydrological cycle over the negro and madeira river basins in the amazon region. *Water*, 10(6), 738. <https://doi.org/10.3390/w10060738>
- Staal, A., Fetzer, I., Wang-Erlandsson, L., Bosmans, J. H. C., Dekker, S. C., Van Nes, E. H., et al. (2020). Hysteresis of tropical forests in the 21st century. *Nature Communications*, 11(1), 4978. <https://doi.org/10.1038/s41467-020-18728-7>
- Stohl, A., Forster, C., Frank, A., Seibert, P., & Wotawa, G. (2005). Technical note: The Lagrangian particle dispersion model flexpart version 6.2. *Atmospheric Chemistry and Physics*, 5(9), 2461–2474. <https://doi.org/10.5194/acp-5-2461-2005>
- Te Wierik, S. A., Keune, J., Miralles, D. G., Gupta, J., Artzy-Randrup, Y. A., Gimeno, L., et al. (2022). The contribution of transpiration to precipitation over African watersheds. *Water Resources Research*, 58(11), e2021WR031721. <https://doi.org/10.1029/2021wr031721>
- Tierney, J. E., Ummenhofer, C. C., & De Menocal, P. B. (2015). Past and future rainfall in the horn of Africa. *Science Advances*, 1(9), e1500682. <https://doi.org/10.1126/sciadv.1500682>
- Tuinenburg, O. A., Theeuwens, J. J. E., & Staal, A. (2020). High-resolution global atmospheric moisture connections from evaporation to precipitation. *Earth System Science Data*, 12(4), 3177–3188. <https://doi.org/10.5194/essd-12-3177-2020>
- Van der Ent, R. J., & Savenije, H. H. G. (2013). Oceanic sources of continental precipitation and the correlation with sea surface temperature. *Water Resources Research*, 49(7), 3993–4004. <https://doi.org/10.1002/wrcr.20296>
- Van der Ent, R. J., Savenije, H. H. G., Schaeffli, B., & Steele-Dunne, S. C. (2010). Origin and fate of atmospheric moisture over continents. *Water Resources Research*, 46(9). <https://doi.org/10.1029/2010wr009127>
- Vellinga, M., & Milton, S. F. (2018). Drivers of interannual variability of the east African “long rains”. *Quarterly Journal of the Royal Meteorological Society*, 144(712), 861–876. <https://doi.org/10.1002/qj.3263>
- Wainwright, C. M., Marsham, J. H., Keane, R. J., Rowell, D. P., Finney, D. L., Black, E., & Allan, R. P. (2019). ‘Eastern African paradox’ rainfall decline due to shorter not less intense long rains. *npj Climate and Atmospheric Science*, 2(1), 34. <https://doi.org/10.1038/s41612-019-0091-7>
- Walker, D. P., Marsham, J. H., Birch, C. E., Scaife, A. A., & Finney, D. L. (2020). Common mechanism for interannual and decadal variability in the east African long rains. *Geophysical Research Letters*, 47(22), e2020GL089182. <https://doi.org/10.1029/2020gl089182>
- Williams, A. P., & Funk, C. (2011). A westward extension of the warm pool leads to a westward extension of the walker circulation, drying eastern Africa. *Climate Dynamics*, 37(11), 2417–2435. <https://doi.org/10.1007/s00382-010-0984-y>
- Yu, L., & Weller, R. A. (2007). Objectively analyzed air–sea heat fluxes for the global ice-free oceans (1981–2005). *Bulletin of the American Meteorological Society*, 88(4), 527–540. <https://doi.org/10.1175/bams-88-4-527>
- Zemp, D. C., Schlessner, C.-F., Barbosa, H. M. J., Hirota, M., Montade, V., Sampaio, G., et al. (2017). Self-amplified amazon forest loss due to vegetation–atmosphere feedbacks. *Nature Communications*, 8(1), 14681. <https://doi.org/10.1038/ncomms14681>